ORIGINAL ARTICLE

Characterization of an 2x2 SCB Optical Switch Integrated with VOA

Hen-Wei Huang and Yao-Joe Yang*

Department of Mechanical Engineering, National Taiwan University, Taiwan

(**Received** 18 September 2011; **Accepted** 23 March 2012; **Published on line** 1 June2012)

*Corresponding author: yjy@ntu.edu.tw

DOI: 10.5875/ausmt.v2i2.107

Abstract: This work presents the modeling, simulation and characterization of an innovative micromachined 2x2 optical switch monolithically integrated with variable optical attenuators. The device uses bi-stable mechanisms for optical switching, and can be easily realized by a standard micromachining process. The split-cross-bar design (SCB) is employed as the optical path configuration. A one-dimensional (1-D) heat transfer model is developed for estimating temperature elevation. An analytical solution is also proposed for the thermo-elastic bending and buckling problem of thermal V-beam and curved beam (pre-shaped buckled beam) actuators. The resulting governing equations with external y-directed force and thermal strain force are solved analytically. Results of the analytical solutions and the finite element (FEM) calculations are compared, with prediction accuracy within 10% of the nonlinear FEM solution, which agrees well with the experimental data.

Keywords: split cross bar; optical switch; converter; variable optical attenuators; analytical

I. Introduction

The recent rapid growth of optical fiber communication networks has boosted demand for various optical components, such as optical switches (OS) [1, 2] and variable optical attenuators (VOA) [3]. In an optical network, OS and VOA are usually deployed together. System complexity and cost increase significantly with the simultaneous use of a large number of single-function switches and attenuators. Therefore, an optical device integrated with switching and attenuating capabilities is desirable to lower the cost and the complexity of optical networks. In this work, we present a novel approach to realize a bi-stable 2x2 OS monolithically integrated with VOAs. The proposed dual-function device can be easily fabricated by a very simple process with a single photo-mask. The key to this approach is the use of the split-cross-bar (SCB) configuration [4, 5] in which all sub-components can be accommodated on a small SOI die without blocking optical paths.

The heat transfer behavior of similar designs has been solved analytically [6-9], but estimating thermo-elastic deformation is primarily accomplished through finite-element methods (FEM) [10-14]. In addition, the analytical model of the bi-stable curved beam is solved in [15]. In this work, we develop an analytical model of the electro-thermo-elastic problems for the V-beam and curved beam actuators with applied external y-directed force and thermal strain force. The temperature of the entire actuator is calculated to accurately determine the tip displacement of the V-beam and curved beam. The results of the analytical solutions and the finite element (FEM) calculations are also compared.

This paper is organized as follows: The device configuration is reviewed in Section II. The analytical models of thermo-elastic behaviors are described in Section III. FEM modeling is presented in Section IV. Section V compares and discusses the results of the analytical models and the FEM approaches, and provides a VOA performance comparison between the measured and modeling results. Finally, Section VI presents conclusions.

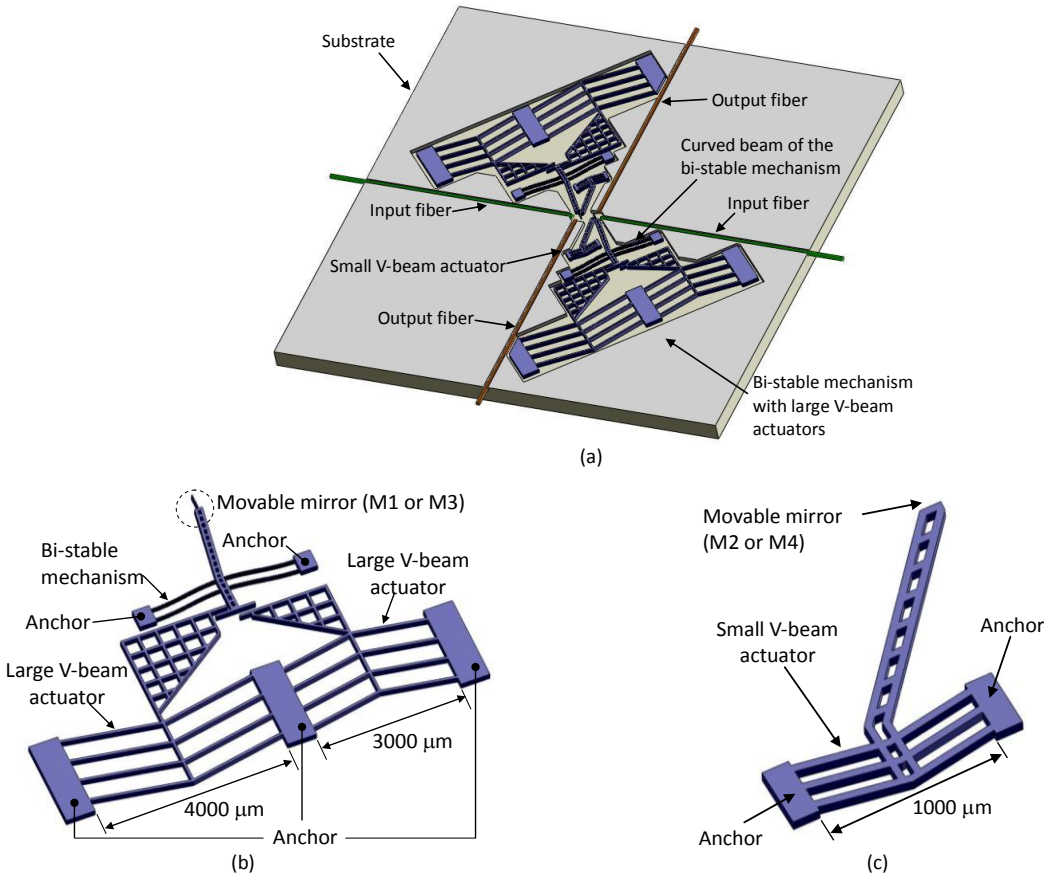

Figure 1. (a) schematic of the dual-function optical device. (b) Enlarged schematic view of the bistable mechanism and the large V-beam actuators used for controlling movable mirrors M1 and M3. (c) Enlarged view of the small V-beam actuator used for controlling movable mirrors M2 and M4.

II. Device configuration

Figure 1 shows the schematic of the dual-function device comprised of two bi-stable mechanisms, two small V-beam actuators, four large V-beam actuators, four fiber grooves, and four input/output fibers. Figure 2 shows the operational principle of the proposed device serving as an OS. As shown in Figure 2(a), four mirrors (i.e., M1, M2, M3 and M4) are used in the OS operation. Figures 2(a) and 2(b) show that optical switching is achieved by moving M1 and M3. Figure 3 illustrates the operational principle of the device operating as a VOA. Figure 3(a) shows the schematic serving as a VOA at OS-State-1. Slightly moving M1 (or M3) in a certain direction (indicated by θ_0) results in misalignment between the reflected light beam and the output channel which, in turn, attenuates optical power. As the displacement of the mirror increases, the optical power decreases. Similarly, Figure 3(b) shows the schematic serving as a VOA at OS-State-2 while Figure 4 shows the SEM pictures of the proposed device realized by a standard DRIE process on an SOI wafer [5].

It is well-known that a relatively large force is required to push the bi-stable mechanism back and forth. One possible method for pushing the mechanism is to use an electro-thermal V-beam actuator [16], which consists of many arched clamped-clamped beams (i.e., the V-structure shown in Figure 5) and undergoes thermal expansion when a current is applied. The arched structure will then deflect toward the arched direction with a large force.

Yao-Joe Joseph YANG received his M.S. and Ph.D. degrees in electrical engineering from the Massachusetts Institute of Technology (MIT EECS) in 1997 and 1999, respectively. Also, he received his M.S. degree (1995) from UCLA and B.S. degree (1990) from NTU, both in mechanical engineering.
From 1999 to 2000, he joined the Coventor Inc, (Cambridge, MA) as a senior application engineer. Since 2000, he joined the Department of Mechanical Engineering at the National Taiwan University, Taipei, Taiwan. Currently he is a professor, and serves as the chair of the department. He is also the director for CAD Technology in the NTU NEMS Center. Since 2009, he serves as the board member of the Chinese Institute of Automation Engineering (CIAE). Currently, he is the secretary general of the Institute.
His research interests include microelectromechanical systems, nanotechnology, high-precision micromachining, flexible sensing arrays, sensor network, parallel processing, and semiconductor devices and vacuum microelectronics modeling. He has been consulted by more than three U.S-based companies and four Taiwan-based organizations. Dr. Yang is a member of IEEE. He is also the recipient of the Outstanding Research Award as well as Dr. Da-Yu Wu Memorial Award (Outstanding Young Researcher Award) of the National Science Council..

Hen-Wei Huang received his B.S. degree in Mechanical Engineering at National Taiwan University, Taiwan in 2011. Currently he is a graduate student in the Mechanical Engineering Department. His research interests include wireless sensor networks, embedded systems for biomedical applications, bi-stable microdevices and microsensors.

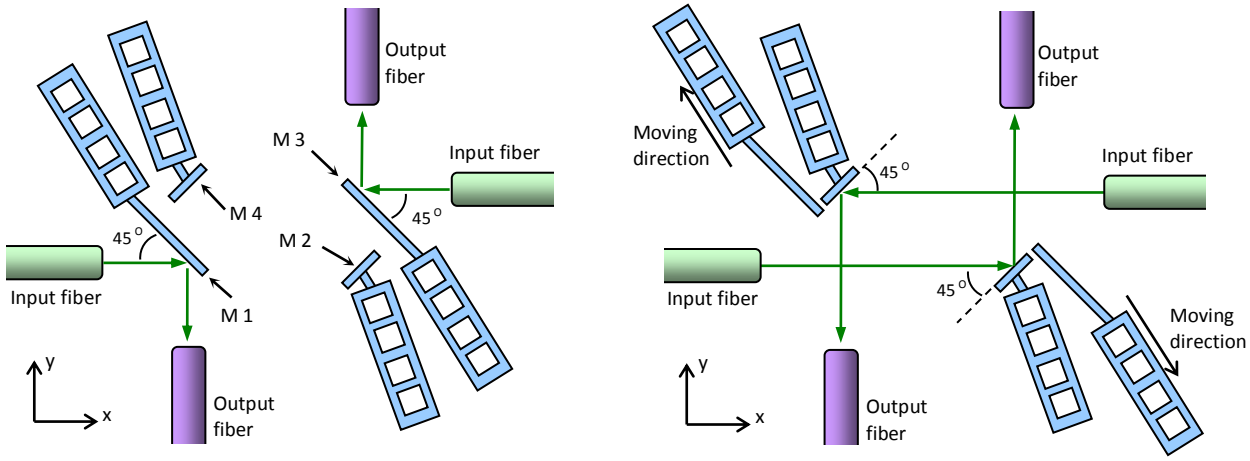

(a) (b)

Figure 2. Operational principle of the dual-function optical device which is operated as an OS (a) OS-State-1: optical signals are reflected by M1 and M3. (b) OS-State-2: M1 and M3 are out of the light path. Optical signals are then reflected by M2 and M4.

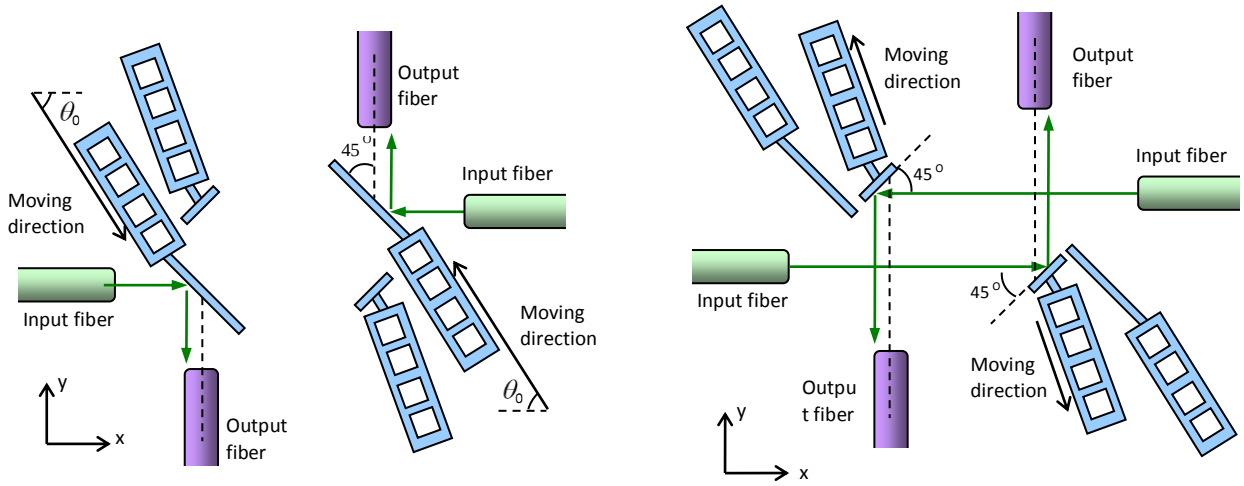

(a) (b)

Figure 3. Operational principle of the dual-function optical device operated as a VOA (a) VOA @ OS-State-1: Optical signals are attenuated by M1 and M3. (b) VOA @ OS-State-2: M1 and M3 are out of the light path. Optical signals are attenuated by M2 and M4.

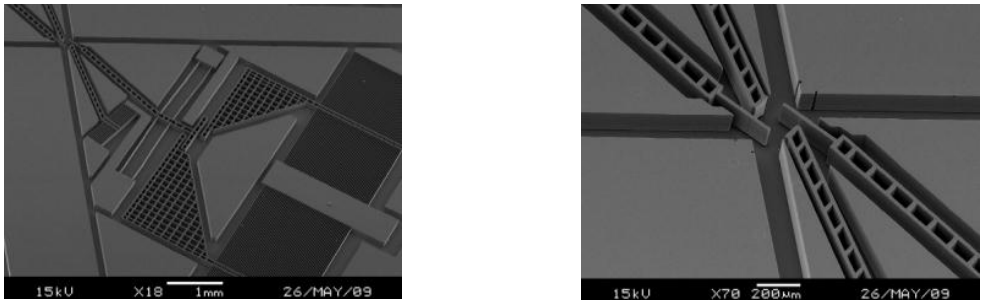

(a) (b)

Figure 4. SEM pictures of the proposed device. (a) Bi-stable mechanism and V-beam actuators, (b) movable mirrors and grooves for lensed fibers.

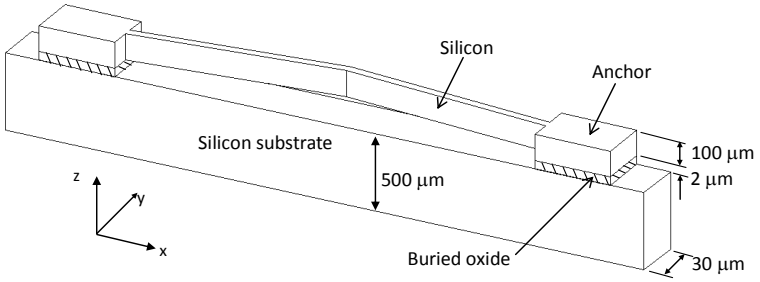

Figure 5. Schematic of the solid model used in the simulation.

III. Thermomechanical Model

A. Heat Transfer Model

To estimate the thermomechanical behavior of the device, we start with the heat transfer effect on the suspended structure. Assuming that convection and radiation effects are negligible, the 1-D heat transfer governing equation [13] for a suspended microstructure over substrate with a volume heat generation by Joule heating is given by:

$$T_{,xx} - \frac{s}{G_u t k_p}(T - T_s) + \frac{v^2}{\rho L^2 k_p} = 0, \quad (1)$$

where G_u is the thermal conductance of air and silicon, k_p is the thermal conductivity, s is the shape factor, t is the thickness, L is the distance between the two anchors of each curved beam actuator, v is the driving voltage, ρ is the specific resistance, and T_s is the substrate temperature (i.e., the anchor temperature). For MEMS devices, the heat flux dissipated toward the substrate (anchor) is significant. The three terms in (1) respectively correspond to the diffusive heat flux along the beam, the heat flux conducted to the substrate, and the volume heating generation (Joule heating). Also, s is the shape factor accounting for the additional heat flux flowing into the substrate across the side walls of the actuator. The schematic of the solid model used in the FEM simulation is shown in Figure 5. An empirical expression for the shape factor for improving the accuracy was reported in [17] as

$$s = 1.685\left[\log\left(\frac{t_{air} + w}{w}\right)\right]^{-0.59}\left(\frac{t_{air}}{t}\right)^{-0.078} L, \quad (2)$$

where t_{air} is the thickness of the air gap between the movable structure and the substrate, and t and w are respectively the thickness and width of the actuator. To simplify the model, thermal conductivity and resistance are assumed to be constant. Since substrate and air layer act as two thermal paths in series, the thermal conductance G_u can be defined as

$$G_u = \frac{t_{air}}{k_{air}} + \frac{t_s}{k_s}, \quad (3)$$

where t_s and k_s are respectively the thickness and thermal conductivity of the substrate. With the boundary conditions of $T(0) = T_s$ and $T_{,x}(L/2) = 0$, the solution for (1) is

$$T(x) - T_s = \frac{\gamma}{k^2}\left[1 - \frac{e^{kx} - e^{k(L-x)}}{1 + e^{kL}}\right], \quad (4)$$

where

$$k^2 = \frac{s}{G_u t k_p}, \quad (5)$$

$$\gamma = \frac{v^2}{\rho L^2 k_p}. \quad (6)$$

Figure 6 shows the temperature comparison by the FEM and the analytical solution. The error between FEM and the analytical model is about 10%. Once the temperature distribution is determined, the tip displacement of the thermal actuators can be estimated using thermal expansion of the beam. The details of the FEM analysis are discussed in next section.

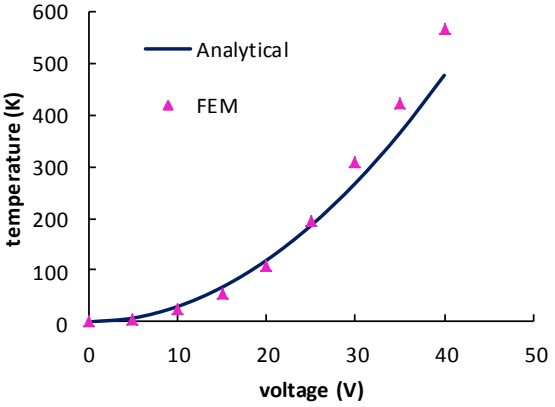

Figure 6. Maximum temperature versus input voltage of the actuator for the V-beam with length of 3000 μm.

B. Curved-beam Actuator

In this work, the curved beam plays two major roles: a bi-stable mechanism for the optical switch, and an in-plane-motion actuator for VOA. When the curved beam serves as a bi-stable mechanism, the governing equation for a curved beam subjected to an axial load P and a y-directed force F on the mid-point is as follows:

$$EI \cdot y_{,xxxx} + P \cdot y_{,xx} = EI \cdot y_{0,xxxx} - F \cdot \delta(x), \quad (7)$$

where E and I are the Young's modulus and the inertia moment of the beam, and $\delta(x)$ is the impulse function. According to the theoretical model [15], the shape of the curved beam is designed as the first buckling mode of a straight beam subjected to an axial load, as shown in Equation (8) and Figure 7(a):

$$y_0 = \frac{h}{2}(1 + \cos k_1 x), \quad (8)$$

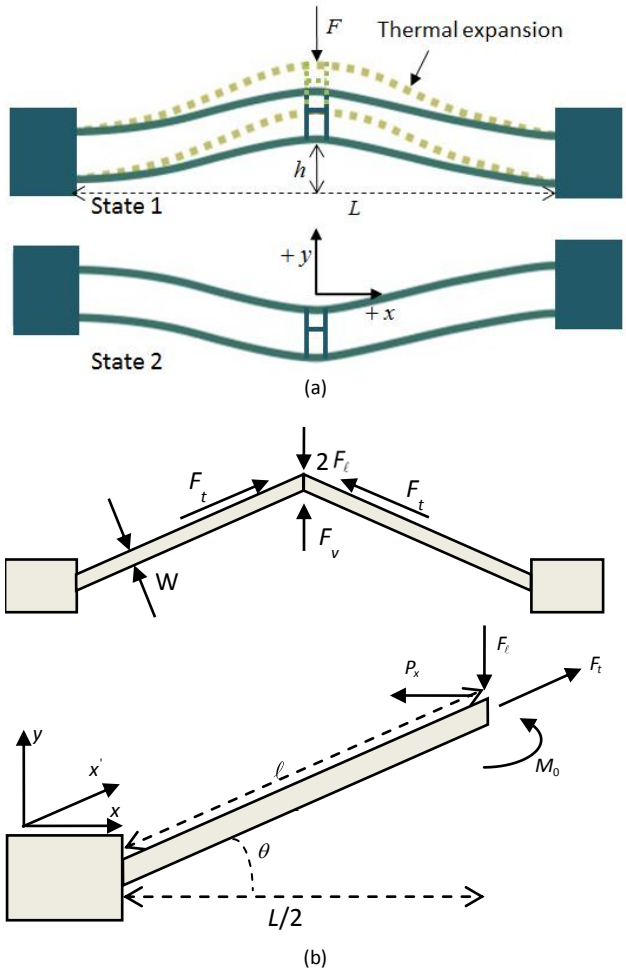

Figure 7. (a) Thermal expansion of the curved beam actuator and the two stable positions (State 1 and State 2). (b) Force diagram of the V-beam actuator.

where $-L/2 \le x \le L/2$, $k_n = 2n\pi/L$, h is the central offset of the curved beam. Also, the shape function satisfies the following boundary conditions: $y_{,x} = 0$ at $x = 0$, $y = y_{,x} = 0$ at $x = -L/2$ and $L/2$. We assume that the shape of the thermally-deformed beam is described by the similar form of Equation (8):

$$y = \sum_{n=1}^{\infty} \frac{w_n}{2} \cdot \left[1 + \cos(k_n x)\right], \tag{9}$$

where w_n is the amplitude of the nth mode. Applying a y-directed force and voltage to the pre-shaped beam generates strain ε and axial force P.

$$\varepsilon = \varepsilon_T + \varepsilon_x = \alpha \cdot \bar{T} - \frac{1}{2L}\int_{-L/2}^{L/2} \left(y_{,x}^2 - y_{0,x}^2\right) dx, \tag{10}$$

where ε_T and ε_x are respectively the thermal strain and the strain due to y-directed force applied to the curved beam. The change of ε gives rise to the axial force P:

$$P = EA\varepsilon = EA \cdot \left[\alpha \cdot \bar{T} - \frac{1}{2L}\int_{-L/2}^{L/2} \left(y_{,x}^2 - y_{0,x}^2\right) dx\right], \tag{11}$$

where

$$\bar{T} = \int_{-L/2}^{L/2} (T(x) - T_s) dx \Big/ L = \frac{\gamma}{k^3 L}\left(kL + 2Cosh\left[\frac{kL}{2}\right] - 2Sinh\left[\frac{kL}{2}\right]\right)$$

is the average temperature increase of the beam. By substituting Equations (8) and (9) into Equation (11), it can be rewritten as

$$P = EA \cdot \left[\alpha \cdot \bar{T} - \frac{1}{4} \cdot \left[\sum_{n=1}^{\infty} \left(\frac{w_n \cdot k_n}{2}\right)^2 - \left(\frac{h \cdot k_1}{2}\right)^2\right]\right]. \tag{12}$$

After substituting the shape functions into the governing equation, we obtain

$$\begin{aligned} &\sum_{n=1}^{\infty}\left[\left(EI \cdot k_n^4 - Pk_n^2\right) \cdot \frac{w_n}{2} \cdot \cos\left(k_n x\right)\right] \\ &= EIk_1^4 \cdot \frac{h}{2} \cdot \cos\left(k_1 x\right) - F \cdot \delta(x) \end{aligned}. \tag{13}$$

By integrating Equation (13) from $x = -L/2$ to $x = L/2$ after multiplying it by $\cos k_1 x$, and employing the orthogonality properties of the eigen-functions, one can derive an analytical form:

$$\left(EI \cdot k_1^4 - P_1 \cdot k_1^2\right) \cdot \frac{w_1 \cdot L}{4} = EI \cdot k_1^4 \left(\frac{hL}{4}\right) - F, \tag{14}$$

where P_1 is the axial force in first mode (n=1). Substituting this into Equation (14), we obtain:

$$F = -\frac{k_1^4 EAL}{64} \cdot \left[w_1^3 + \left(\frac{16I}{A} - \left(\frac{16\alpha\bar{T}}{k_1^2} + h^2\right)\right) w_1 - 16\frac{Ih}{A}\right]. \tag{15}$$

Under a special condition of zero loading (i.e., $F = 0$), we obtain

$$w_1^3 + \left(\frac{16I}{A} - \left(\frac{16\alpha\bar{T}}{k_1^2} + h^2\right)\right) w_1 - 16\frac{Ih}{A} = 0. \tag{16}$$

The curved beam expands due to Joule heating as shown in Figure 7(a). Solving Equation (16), we obtain two stable positions of the bistable mechanism, which are indicated in Figure 8(a). The first stable position due to thermal expansion can be shown as

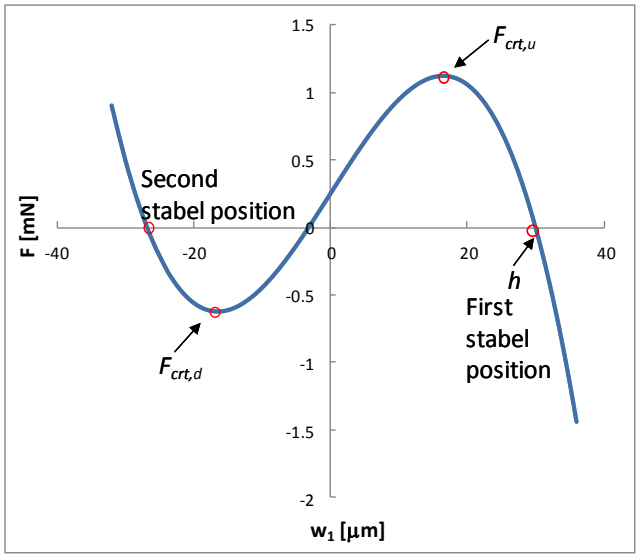

(a)

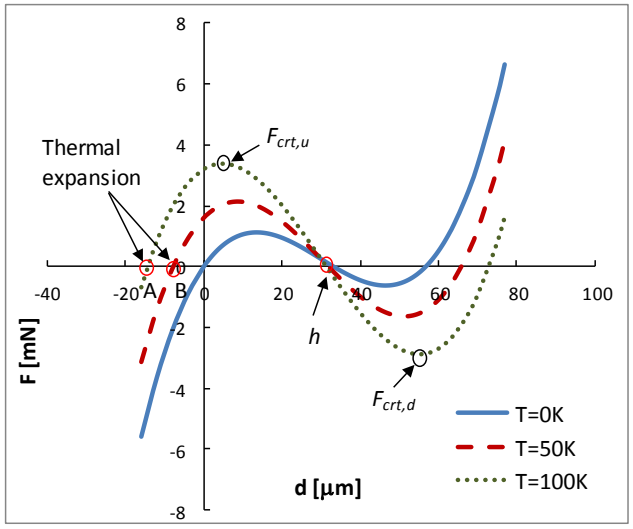

(b)

Figure 8. (a) Applied external y-directed force (F_ℓ) versus the first mode of curved beam. (b) Applied external force versus deformation ($d = h - w_1$) at different average temperatures of the curved beam.

$$w_{fst} = \sqrt[3]{-b/2 + \sqrt{b^2/4 + a^3/27}} - \sqrt[3]{b/2 + \sqrt{b^2/4 + a^3/27}}, \quad (17)$$

where $a = \frac{16I}{A} - \left(\frac{16\alpha\bar{T}}{k_1^2} + h^2\right)$ and $b = -16\frac{Ih}{A}$, which corresponds with the results in [18]. Figure 8(b) shows the applied external force versus the amplitude of the deformation $(d = h - w_1)$ at different average temperature $\bar{T}$ of the curved beam. Note that the points in A and B indicate the amplitudes due to thermal expansion without applying external force (the displacement of the first stable position) given respective average temperatures of 50 K and 100 K. The amplitude of the first mode (n=1) at the critical positions can be derived by solving $dF/dw_1 = 0$ [19]:

$$w_{1,crt} = \pm\sqrt{\frac{16I}{3A} - \frac{16\alpha\bar{T} + k_1^2 h^2}{3k_1^2}}. \quad (18)$$

Substituting the two critical positions of Equation (18) into Equation (15), the critical external y-directed forces can be found at the local maximum and local minimum (see Figure 8(a)):

$$F_{crt,d} = -\frac{k_1^4 EAL}{64} \cdot \left[\left(\frac{16I}{3A} - \frac{16\alpha\bar{T} + k_1^2 h^2}{3k_1^2}\right)^{3/2} \cdot \left(\frac{\sqrt{3}+1}{\sqrt{3}}\right) - \frac{16Ih}{A}\right] \quad (19)$$

and

$$F_{crt,u} = \frac{k_1^4 EAL}{64} \cdot \left[\left(\frac{16I}{3A} - \frac{16\alpha\bar{T} + k_1^2 h^2}{3k_1^2}\right)^{3/2} \cdot \left(\frac{\sqrt{3}+1}{\sqrt{3}}\right) + \frac{16Ih}{A}\right]. \quad (20)$$

In the analytical model, the two stable positions and the critical force are dependent on the average temperature. As shown in Figure 8(b), increases in the average temperature increase the distance between the two stable positions and the critical forces [20].

C. V-beam Actuator

When applying voltage on the anchors of the V-beam actuator, the two arms expand and push the tip along the y-axis, as shown in Figure 7(b). Being symmetric, the two arms can be considered to be two fixed-guided beams. The guided end of each arm moves along the y-axis. The boundary conditions of the guided end, including a reactive force (P_x), a reactive moment (M_0), a virtual force applied on y-directed direction (F_v) and a y-directed applied force (F_ℓ), are also shown in Figure 7(b). In addition, the thermal force F_t due to the elongation of the arm by heating can be modeled as:

$$F_t = EA \cdot \varepsilon_T = EA\alpha\bar{T}. \quad (21)$$

The bending moment around the z-axis (M_z) and the axial force (F_x) can be written as

$$F_{x'} = F_t - P_x \cdot \cos\theta + F_v \cdot \sin\theta - F_\ell \cdot \sin\theta , \quad (22)$$

$$M_z = M_o + F_v \cdot x' \cos\theta - F_\ell \cdot x' \cdot \cos\theta + P_x \cdot x' \sin\theta . \quad (23)$$

The strain energy U_p due to the axial force $F_{x'}$ can be calculated as

$$U_p = \frac{1}{2EA}\int_0^\ell F_{x'}^2 dx' = \frac{\left[F_t - P_x\cos\theta + (F_v - F_\ell)\sin\theta\right]^2 \cdot l}{2EA} . \quad (24)$$

The strain energy U_b due to the bending moment can be calculated as

$$\begin{aligned} U_b &= \frac{1}{2EI}\int_0^\ell M_z^2 dx' \\ &= \frac{1}{2EI}\int_0^\ell \left[M_o + (F_v - F_\ell)x' \cdot \cos\theta + P_x \cdot x' \cdot \sin\theta\right]^2 dx' \end{aligned} . \quad (25)$$

Finally, the total strain energy in the system is:

$$U_t = U_p + U_b , \quad (26)$$

where θ is the incline angle of the arm and ℓ is the half length of the v-beam actuator.

The boundary conditions at the guided end provide the required equations for the analytical solution. The x-displacement u_x and rotation around the z-axial θ_z are both zero at the guided end. Then, applying Castigliano's displacement theorem, the following equations are obtained

$$u_x = 0 \Rightarrow \frac{\partial U_t}{\partial P_x} = 0 , \quad (27)$$

$$\theta_z = 0 \Rightarrow \frac{\partial U_t}{\partial M_o} = 0 . \quad (28)$$

Using the above two equations, P_x and M_o can be expressed in terms of F_t, F_ℓ and the geometrical parameters of the actuator. Then, the y-displacement of the arm Δy can be calculated by applying a virtual force F_v in y-direction at the free end of the beam.

$$P_x = \frac{12EI \cdot F_t \cos\theta + \frac{1}{2}\left(EAl^2 - 12EI\right)F_\ell \sin 2\theta}{12EI\cos^2\theta + EAl^2\sin^2\theta} , \quad (29)$$

$$M_o = \frac{l}{2}\left(F_\ell\cos\theta - P_x\sin\theta\right) . \quad (30)$$

Applying Castigliano's theorem and setting the virtual force to zero ($F_v = 0$) yields

$$\begin{aligned} \Delta y &= \frac{\partial U_t}{\partial F_v} \\ &= \frac{\left(F_t - P_x\cos\theta - F_\ell\sin\theta\right)l\sin\theta}{EA} \\ &\quad + \frac{M_o l^2\cos\theta + \frac{l^3}{3}\left(P_x\sin 2\theta\right) - 2F_\ell\cos^2\theta}{2EI} \end{aligned} . \quad (31)$$

Substituting P_x and M_o into Equation (29) yields a simple relationship between the thermal strain force, y-directed applied force and tip displacement.

$$\Delta y = \frac{\left(F_t\sin\theta - F_\ell\right)l^3}{12EI\cos^2\theta + EAl^2\sin^2\theta} . \quad (32)$$

Note that if the external y-directed force $F_\ell = 0$, Equation (32) is the same as in [21].

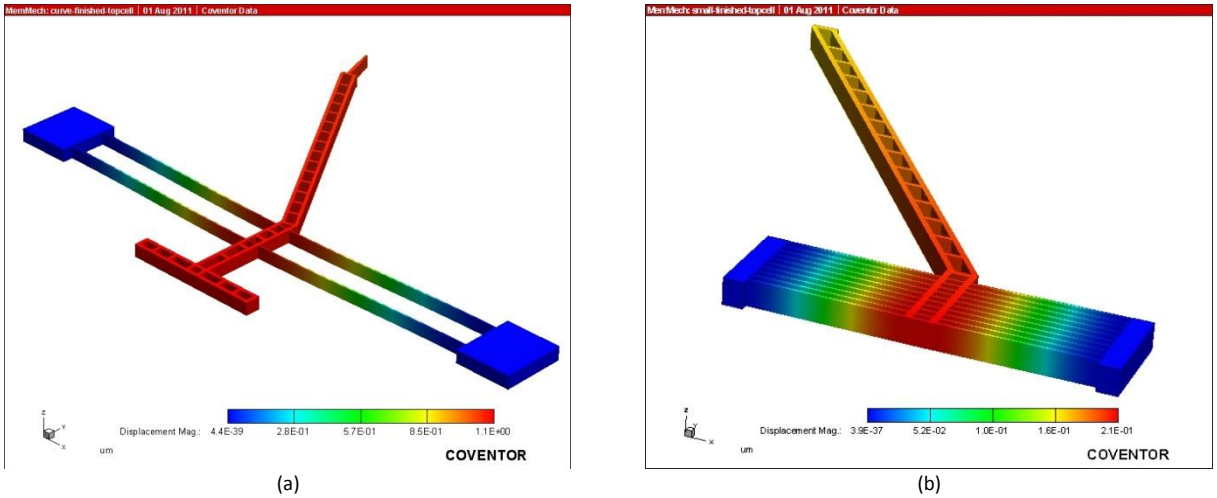

(a) (b)

Figure 9. Simulated displacement of the structure when applying a voltage of 5V: (a) curved beam, (b) small V-beam.

Table I. Dimensions of the bi-stable mechanism and the V-beam actuator.

Bi-stable mechanism	
Distance between two anchors (*L*)	3000 μm
Curved beam width (*W*)	8 μm
Central offset (*h*)	30 μm
V-beam actuator	
Half beam length (ℓ)	1000, 1500, 2000 μm
Beam width (*W*)	10 μm
Inclined angle (θ)	0.6°

Table II. Material properties used in the simulations of the V-structure.

Parameter	Material	Value
Young's modulus (GPa)	Si	169
	SiO_2	73
Density ($kg\ m^{-3}$)	Si	2330
	SiO_2	2200
Poisson's ratio	Si	0.28
	SiO_2	0.17
Thermal conductivity, K ($W\ m^{-1}K^{-1}$)	Si	Table III
	SiO_2	1.4
	Air	0.03
Thermal expansion coefficient, α_T ($\times 10^{-6} K^{-1}$)	Si	Table III
	SiO_2	0.4
Specific heat, C_P ($J\ kg^{-1}\ K^{-1}$)	Si	Table III
	SiO_2	1000
Resistivity (Ω cm)	Si	0.5

Table III. Temperature dependence of the thermal conductivity (k), thermal expansion coefficient (α_T), and specific heat (C_p) for single-crystal silicon.

Temperature (K)	k ($Wm^{-1}K^{-1}$) [22]	α_T ($\times 10^{-6} K^{-1}$) [23]	C_P ($J\ kg^{-1}\ K^{-1}$) [24]
300	156	2.614	732
400	105	3.253	794
500	80	3.614	857
600	64	3.842	878
700	52	4.016	899
800	43	4.151	911

IV. Results and Discussions

The thermal-mechanical behavior of the V-beam and curved beam actuator were also simulated using the commercial FEM package CoventorWare™ using 3D models. Figure 5 shows the schematic of the simulated model of a V-structure. For electro-thermal analysis, a voltage difference was applied between the anchors of the actuator. The temperature of the substrate bottom was fixed at constant temperature, and a convection boundary condition was applied for all surfaces. For thermo-mechanical analysis, the bottom surfaces of the anchors were fixed on the substrate surfaces. The electro-thermal analysis computed the temperature distributions of the structure. The temperature distributions were then used as the volume conditions for the thermo-mechanical analysis to calculate structural deformations.

Figure 9 shows the simulated results of the thermal actuator with an applied voltage of 5 V. The dimensions of the curved beam and v-beam actuators used in the FEM simulations and analytical models are presented in Table I. All the thermal properties and the material constants can be found in Tables II and III. The calculated tip displacements for different V-beam structures (1000 μm, 3000 μm and 4000 μm in length) are shown in Figures 10(b) and 11, which also show the results by the analytical solution of Equations (17) and (32) without applied external y-directed force. FEM simulations and measured displacements at different input voltages for the V-beam and curved-beam actuators are also shown. Figures 10(a) and (b) show the tip displacement versus input voltage for the curved beam and small V-beam actuator with respective beam lengths of 3000 μm and 1000 μm. Figures 11(a) and (b) show the tip displacement versus input voltage for the large V-beam actuator with respective beam lengths of 4000 μm and 3000 μm. The tip displacement is seen to increase with the beam length. Figure 12 shows the analytical solution of Equation (32) and the semi-analytical solution from [10] with an applied y-directed force of $F_\ell = 1000\mu N$. All the parameters used in Figure 12 are the same as those used in [10].

Figure 13 illustrates the measured and analytical attenuation performance versus applied voltages, showing good agreement between the measured results and the analytical results for state 1 and state 2 with different angles. Note that the analytical attenuation is calculated from the displacement of the mirror [25]. For the VOA@OS-State-1, the measured attenuation reaches 33 dB under an applied voltage of 20 V. For the VOA@OS-State-2, an attenuation of 34 dB can be achieved with 15 V. The measured results are in a good agreement with the calculated results.

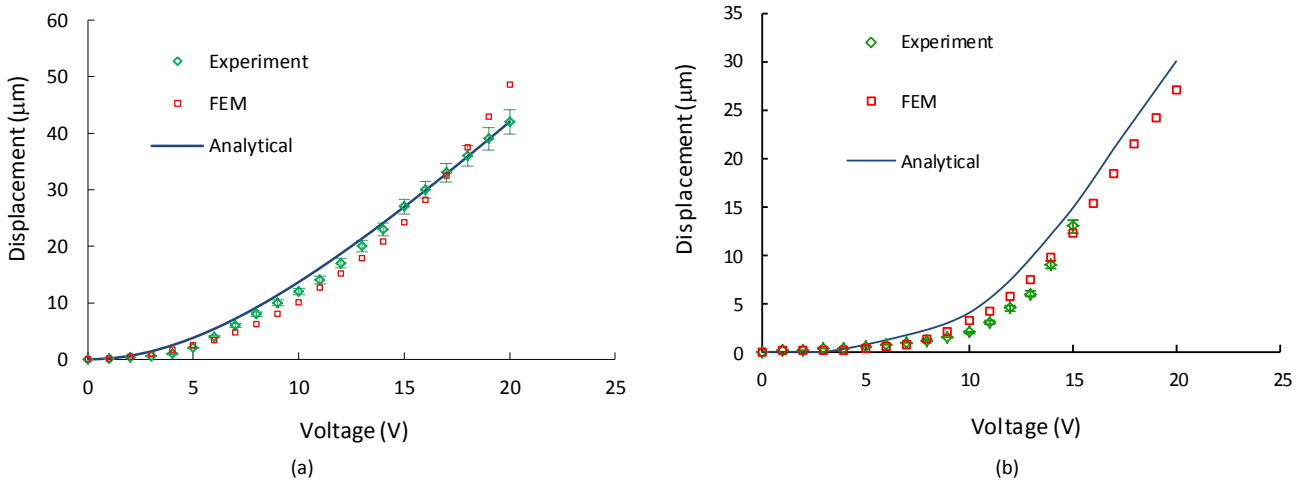

Figure 10. Tip displacement versus input voltage of the actuators for: (a) curved beam, (b) small V-beam actuator with length of 1000 μm.

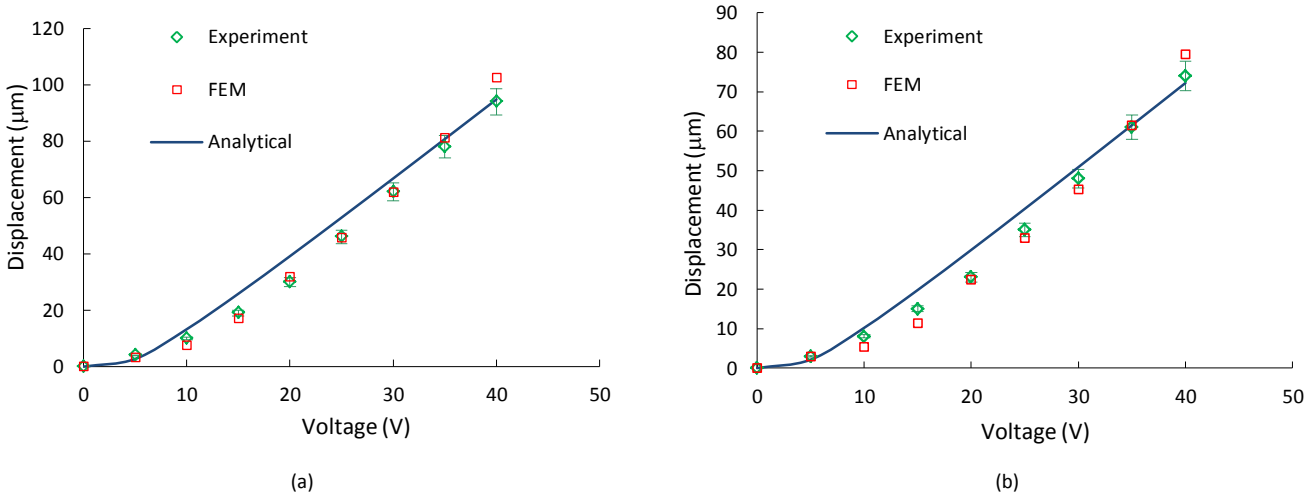

Figure 11. Tip displacement versus input voltage of the actuators for: (a) large V-beam actuator with beam length of 4000 μm and (b) large V-beam actuator with beam length of 3000 μm.

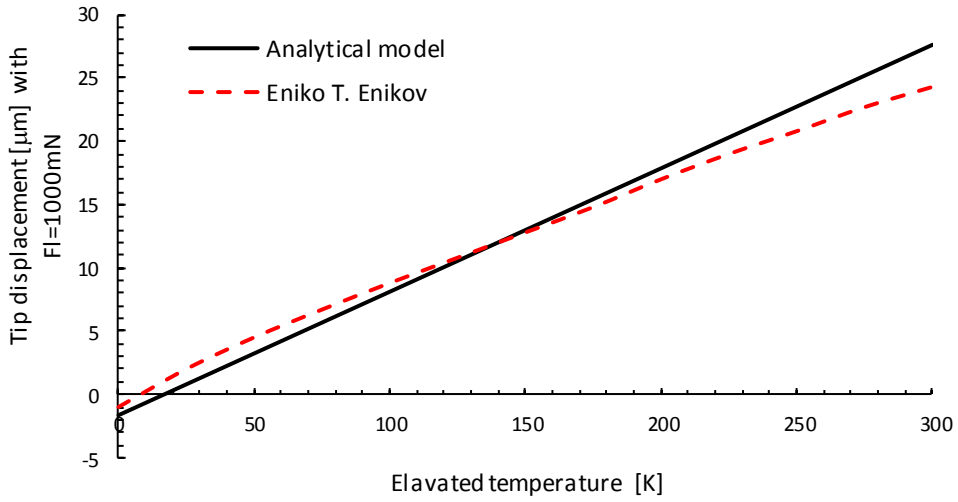

Figure 12. Tip displacement of the v-beam actuator with applied external force $F_i = 1000\mu N$ compared with the semi-analytical solution of Enikov [10].

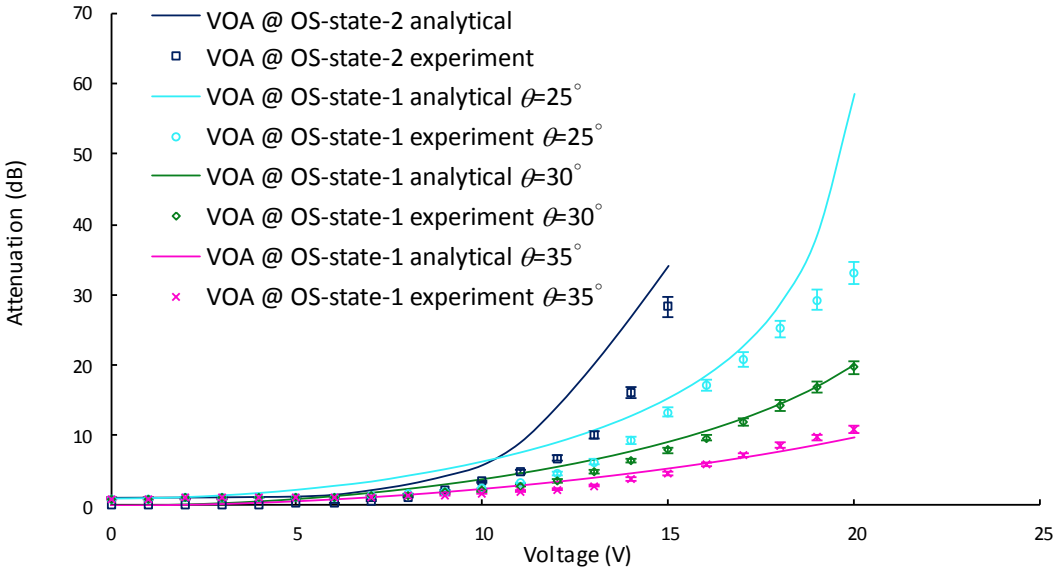

Figure 13. Measured and analytical attenuation versus different driving voltages.

V. Conclusion

This work presents the modeling, simulation and characterization of an MEMS optical device. The modeled device is fully-monolithically integrated using micromachining techniques and has dual functions: optical switching and variable optical attenuating. A curved beam bi-stable mechanism is adopted for optical switching, and the split-cross-bar design (SCB) is used as the optical path configuration. Analytical solutions of the thermo-elastic bending and buckling of the microstructures in the device are proposed. The results predicted by the analytical solutions are compared with the finite element (FEM) calculated results, with a discrepancy of under 10%. The experimental results are also in a good agreement with theoretical predictions, which suggests that the analytical modeling results presented in this work are useful for applications in MEMS devices with curved beam bi-stable structures.

Acknowledgement

This work was supported in part by the National Science Council, Taiwan, R.O.C. (Contract No: NSC 94-2212-E-002-060). The authors would like to thank Mr. Sun-Chih Shih and Mr. Shen-An Yang for their help on the packaging process.

References

[1] W. Li, J. Liang, Z. Liang, X. Li, W. Wang, Y. Zhong, and D. Sun, "Design and fabrication of a micro-optic switch," *Optical Express,* vol. 16, no. 9, pp. 6324-6330, 2008.
doi: 10.1364/OE.16.006324

[2] A. Groisman, S. Zamek, K. Campbell, L. Pang, U. Levy, and Y. Fainman, "Optofluidic 1x4 switch," *Optical Express,* vol. 16, no. 18, pp. 13499-13508, 2008.
doi: 10.1364/OE.16.013499

[3] X. M. Zhang, Q. W. Zhao, A. Q. Liu, J. Zhang, J. H. Lau, and C. H. Kam, "Asymmetric tuning schemes of MEMSdual-shutter VOA," *Journal of Lightwave Technology,* vol. 26, no. 5, pp. 569-579, 2008. Avaliable: http://jlt.osa.org/abstract.cfm?URI=jlt-26-5-569

[4] B. T. Liao, H. H. Shen, H. H. Liao, and Y. J. Yang, "A bi-stable 2x2 optical switch monolithically integrated with variable optical attenuators," *Optical Express,* vol. 17, no. 22, pp. 19919-19925, 2009.
doi: 10.1364/OE.17.019919

[5] Y. J. Yang, B. T. Liao, and W. C. Kuo, "A novel 2 × 2 mems optical switch using the split cross-bar design," *Journal of Micromechanics and Microengineering,* vol. 17, no. 5, pp. 875-882, 2007.
doi: 10.1088/0960-1317/17/5/005

[6] Q. A. Huang and N. K. S. Lee, "Analysis and design of polysilicon thermal flexure actuator," *Journal of Micromechanics and Microengineering,* vol. 9, no. 1, pp. 64-70, 1999.
doi: 10.1088/0960-1317/9/1/308

[7] L. Que, J. S. Park, and Y. B. Gianchandani, "Bent-beam electrothermal actuators-part I: Single beam and cascaded devices," *Microelectromechanical Systems, Journal of,* vol. 10, no. 2, pp. 247-254, 2001.
doi: 10.1109/84.925771

[8] D. Yan, A. Khajepour, and R. Mansour, "Modeling of two-hot-arm horizontal thermal actuator," *Journal of Micromechanics and Microengineering,* vol. 13, no. 2, pp. 312-322, 2003. doi: 10.1088/0960-1317/13/2/321

[9] R. Hickey, D. Sameoto, T. Hubbard, and M. Kujath, "Time and frequency response of two-arm micromachined thermal actuators," *Journal of Micromechanics and Microengineering,* vol. 13, no. 1, pp. 40-46, 2003. doi: 10.1088/0960-1317/13/1/306

[10] E. T. Enikov, S. S. Kedar, and K. V. Lazarov, "Analytical model for analysis and design of V-shaped thermal microactuators," *Microelectromechanical Systems, Journal of,* vol. 14, no. 4, pp. 788-798, 2005. doi: 10.1109/JMEMS.2005.845449

[11] C. D. Lott, "Electrothermomechanical modeling of a surface-micro-machine linear displacement microactuator," M.S. Thesis, Brigham Young University, 2001.

[12] M. Baltzer, T. Kraus, and E. Obermeier, "A linear stepping actuator in surface micromachining technology for low voltages and large displacements," in *International Conference on Solid-State Sensors and Actuators*, Chicago, 1997, pp. 781 -784. doi: 10.1109/SENSOR.1997.635216

[13] C. D. Lott, T. W. McLain, J. N. Harb, and L. L. Howell, "Modeling the thermal behavior of a surface-micromachined linear-displacement thermomechanical microactuator," *Sensors and Actuators A: Physical,* vol. 101, no. 1–2, pp. 239-250, 2002. doi: 10.1016/S0924-4247(02)00202-9

[14] J. H. Comtois, V. M. Bright, and M. W. Phipps, "Thermal microactuators for surface-micromachining processes," *Proceedings of SPIE,* vol. 2642, no. 1, pp. 10-21, 1995. doi: 10.1117/12.221154

[15] J. Qiu, J. H. Lang, and A. H. Slocum, "A curved-beam bistable mechanism," *Microelectromechanical Systems, Journal of,* vol. 13, no. 2, pp. 137-146, 2004. doi: 10.1109/JMEMS.2004.825308

[16] C. Lee and C. Y. Wu, "Study of electrothermal v-beam actuators and latched mechanism for optical switch," *Journal of Micromechanics and Microengineering,* vol. 15, no. 1, pp. 11-19, 2005. doi: 10.1088/0960-1317/15/1/003

[17] J. E. Sunderland and K. R. Johnson, "Shape factors for heat conduction through bodies with isothermal or convective boundary conditions," *ASHRAE Transactions,* vol. 70, pp. 237-241, 1964. Available: http://poplab.ece.illinois.edu/files/ece598/SunderlandShapeFactorsTABLE-ashrae64.pdf

[18] W. Fang and J. A. Wickert, "Post buckling of micromachined beams," *Journal of Micromechanics and Microengineering,* vol. 4, no. 3, pp. 116-122, 1994. doi: 10.1088/0960-1317/4/3/004

[19] S. Park and D. Hah, "Pre-shaped buckled-beam actuators: Theory and experiments," *Sensors and Actuators A: Physical,* vol. 148, no. 1, pp. 186-192, 2008. doi: 10.1016/j.sna.2008.07.009

[20] Y. Gerson, S. Krylov, and B. Ilic, "Electrothermal bistability tuning in a large displacement micro actuator," *Journal of Micromechanics and Microengineering,* vol. 20, no. 11, pp. 112001-112001, 2010. doi: 10.1088/0960-1317/20/11/112001

[21] C. Elbuken, L. Gui, C. L. Ren, M. Yavuz, and M. B. Khamesee, "Design and analysis of a polymeric photo-thermal microactuator," *Sensors and Actuators A: Physical,* vol. 147, no. 1, pp. 292-299, 2008. doi: 10.1016/j.sna.2008.04.019

[22] C. J. Glassbrenner and G. A. Slack, "Thermal conductivity of Silicon and Germanium from 3°K to the melting point," *Physical Review,* vol. 134, no. 4A, pp. A1058-A1069-A1058-A1069, 1964. doi: 10.1103/PhysRev.134.A1058

[23] R. B. Roberts, "Thermal expansion reference data: Silicon 300-850 K," *Journal of Physics D: Applied Physics,* vol. 14, no. 10, pp. L163-L166, 1981. doi: 10.1088/0022-3727/14/10/003

[24] A. Goldsmith, T. E. Waterman, and H. J. Hirschhorn, *Handbook of thermophysical properties of solid materials.* Oxford: Pergamon Pr., 1961.

[25] C. H. Kim, N. Park, and Y. K. Kim, "MEMS reflective type variable optical attenuator using off-axis misalignment," 2002, pp. 55-56. doi: 10.1109/OMEMS.2002.1031440